Stem Cell Reports
Article

ISSCR

OPEN ACCESS

Unusual X chromosome inactivation maintenance in female alveolar type 2 cells is correlated with increased numbers of X-linked escape genes and sex-biased gene expression

Isabel Sierra,[1,6] Sarah Pyfrom,[1,6] Aaron Weiner,[1] Gan Zhao,[1] Amanda Driscoll,[1] Xiang Yu,[3] Brian D. Gregory,[2] Andrew E. Vaughan,[1,4,5,*] and Montserrat C. Anguera[1,4,*]

[1]Department of Biomedical Sciences, School of Veterinary Medicine, University of Pennsylvania, Philadelphia, PA, USA
[2]Department of Biology, University of Pennsylvania, Philadelphia, PA, USA
[3]Joint International Research Laboratory of Metabolic & Developmental Sciences, School of Life Sciences and Biotechnology, Shanghai Jiao Tong University, Shanghai 200240, China
[4]Institute for Regenerative Medicine, University of Pennsylvania, Philadelphia, PA 19104, USA
[5]Penn Lung Biology Institute, University of Pennsylvania, Philadelphia, PA 19104, USA
[6]These authors contributed equally
*Correspondence: anguera@vet.upenn.edu (M.C.A.), vaughan@vet.upenn.edu (A.E.V.)
https://doi.org/10.1016/j.stemcr.2022.12.005

SUMMARY

Sex differences exist for many lung pathologies, including COVID-19 and pulmonary fibrosis, but the mechanistic basis for this remains unclear. Alveolar type 2 cells (AT2s), which play a key role in alveolar lung regeneration, express the X-linked *Ace2* gene that has roles in lung repair and SARS-CoV-2 pathogenesis, suggesting that X chromosome inactivation (XCI) in AT2s might impact sex-biased lung pathology. Here we investigate XCI maintenance and sex-specific gene expression profiles using male and female AT2s. Remarkably, the inactive X chromosome (Xi) lacks robust canonical Xist RNA "clouds" and less enrichment of heterochromatic modifications in human and mouse AT2s. We demonstrate that about 68% of expressed X-linked genes in mouse AT2s, including *Ace2*, escape XCI. There are genome-wide expression differences between male and female AT2s, likely influencing both lung physiology and pathophysiologic responses. These studies support a renewed focus on AT2s as a potential contributor to sex-biased differences in lung disease.

INTRODUCTION

COVID-19, the disease caused by SARS-CoV-2, commonly presents as pneumonia, with those most severely affected progressing to acute respiratory distress syndrome (ARDS) (CDC COVID-19 Response Team, 2020), itself bearing a mortality rate as high as 45%. As previously observed with related coronaviruses SARS-CoV and MERS (Channappanavar et al., 2017), older males are at significantly higher risk for severe or fatal outcomes from COVID-19 (Chen et al., 2020; Galbadage et al., 2020; Lau et al., 2021; Peckham et al., 2020; Takahashi et al., 2020; Wenham et al., 2020). Since the onset of the pandemic, this male sex bias is incredibly consistent across the globe, with increases in mortality among older genetic (XY) males (Galbadage et al., 2020; Lau et al., 2021; Peckham et al., 2020; Takahashi et al., 2020). A greater understanding of the underlying mechanisms contributing to this male bias may reveal novel insights for the treatment or reduction of disease severity.

Severe COVID-19/ARDS is characterized by diffuse alveolar damage, wherein large regions of alveolar epithelium are ablated either directly by SARS-CoV-2 infection or indirectly by virus-induced inflammatory stresses (e.g., "cytokine storms"). Within the alveolar parenchyma, alveolar type 2 cells (AT2s), responsible for pulmonary surfactant production, are also extremely well characterized as alveolar progenitor cells. Upon injury, AT2s can proliferate, restore the loss of surfactant-producing cells, and differentiate to re-establish gas-exchanging alveolar type I cells (AT1s) (Barkauskas et al., 2013; Evans et al., 1975). Whether any of the sex differences in COVID-19 might reflect sex differences within alveolar progenitor cells themselves has not been explored. However, there have been a few developmental studies that report sex differences in cell number and functionality of fetal lung epithelial cells, surfactant phospholipid content in fetal rat lungs, and expression of apolipoprotein genes in fetal lung RNA (Kaltofen et al., 2015; McCoy et al., 1999; Simard et al., 2006). To date, there are no unbiased investigations of genome-wide transcriptional profiling of male and female AT2s.

Female mammals use X chromosome inactivation (XCI) to equalize expression of X-linked genes between the sexes. XCI is initiated during female embryonic development by the expression of the long non-coding RNA Xist (Marahrens et al., 1997; Penny et al., 1996), which recruits chromatin modifiers that deposit heterochromatic histone modifications across the entire X chromosome, resulting in allele-specific gene silencing (Kohlmaier et al., 2004; Yildirim et al., 2013; Zhao et al., 2008). *Xist* deletion or loss in hematopoietic stem cells and human pluripotent stem cells results respectively in partial X-reactivation with increased expression of certain X-linked genes, dependent on cell type (Yildirim et al., 2013) (Anguera et al., 2012;

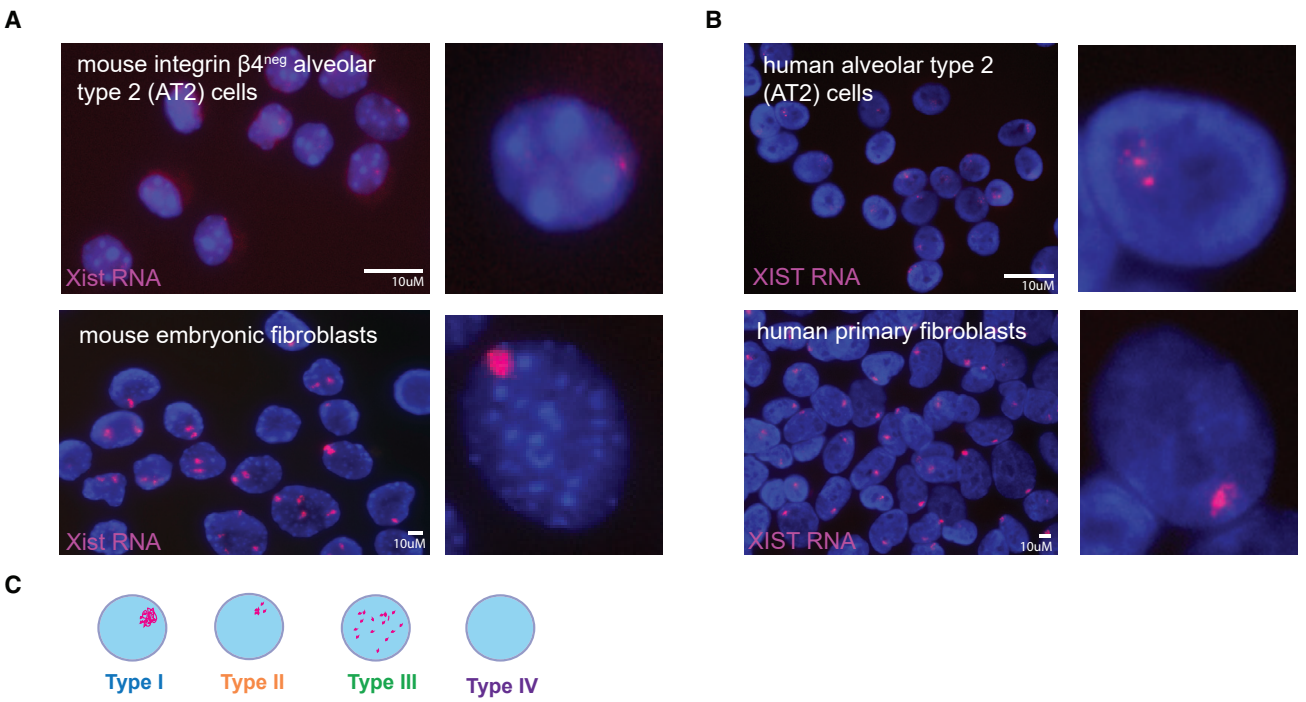

(legend on next page)

Mekhoubad et al., 2012). While XCI has been considered a stable attribute of female somatic cells, we have found that XCI in lymphocytes is unusually dynamic. Our research found that mature lymphocytes from female mice and humans lack Xist RNA "clouds" and enrichment of heterochromatic marks on the inactive X chromosome (Xi) and that these epigenetic modifications return in stimulated lymphocytes (Syrett et al., 2017, 2019; Wang et al., 2016). We also discovered that other immune cells have dispersed Xist RNA localization patterns (Syrett et al., 2018). Whether atypical XCI maintenance extends to additional cell types that could contribute to sex-biased differences in COVID severity is unknown.

Interestingly, the X chromosome encodes angiotensin-converting enzyme 2 (*ACE2*), an enzyme centrally involved in multiple aspects of SARS-CoV-2 pathogenesis, including acting as the major viral receptor (Huang et al., 2020; Katsura et al., 2020). However, because ACE2 also plays an important role in degradation of bradykinin and angiotensin II (which contributes to lung injury), it is difficult to predict how increased or decreased levels of ACE2 contribute to disease severity beyond the minimal expression level required for initial infection (Imai et al., 2005). Indeed, *Ace2* knockout mice exhibit much more severe lung injury after acid aspiration and H5N1 influenza infection, while administration of recombinant Ace2 is protective (Imai et al., 2005; Zou et al., 2014). Thus, if *ACE2* "escapes" XCI in AT2s, it is unclear how this might affect pathophysiology upon SARS-CoV-2 infection.

Here we assessed whether AT2s might, like lymphocytes, exhibit non-canonical XCI maintenance, and whether this might contribute toward sex-biased expression of both X-linked and autosomal genes. We find that AT2s from mouse and human lungs lack the canonical robust Xist "clouds" typical of somatic cells and exhibit very low enrichment of two heterochromatic modifications, H3K27me3 and H2AK119-ubiquitin, on the Xi. Allele-specific quantification of the Xi revealed that about 50% of the X-linked genes expressed in AT2 cells "escape" XCI in adult mouse AT2s. Finally, we performed whole-transcriptome differential expression analysis, observing a strikingly large number of gene expression differences between male and female AT2s, which likely contribute to sex differences in lung injury and repair in multiple settings including COVID-19.

RESULTS

Female AT2 cells have faint and dispersed Xist RNA pinpoints

To isolate AT2 cells from adult female mouse lungs, we gated on CD45^{neg} Epcam^{pos} Integrin β4^{pos} cells, as we previously demonstrated that this sort scheme results in >96% enrichment for AT2s (Chapman et al., 2011; Vaughan et al., 2015; Weiner et al., 2019). Consistent with previous results, sorted cells were approximately 99% pure (Figure S1). AT2 cells were immediately cytospun and fixed, and used for Xist RNA fluorescence *in situ* hybridization (RNA FISH) using oligo probes specific for repetitive regions within Xist RNA (Syrett et al., 2017). Surprisingly, unlike transformed mouse embryonic fibroblasts (MEFs) which have robust Xist RNA "clouds," female mouse AT2 cells had very faint pinpoints of Xist RNA or completely lacked Xist RNA signals (Figure 1A). Mouse AT2 cells contained two Xs using X-paints for DNA FISH, and Xist pinpoints could identify the Xi in some cells (Figure S1D). To determine whether human female AT2 cells also lacked robust XIST RNA localization at the Xi, we isolated human AT2 cells from explanted lungs of healthy donors as previously described, utilizing the AT2-specific HTII-280 antibody (Xi et al., 2017). Sorted human AT2 cells were used for XIST RNA FISH using human-specific oligo probes (Wang et al., 2016), and these cells also exhibited pinpoints of XIST RNA, instead of robust XIST RNA signals typical of human fibroblasts (Figure 1B). Human AT2 cells also contained two X chromosomes, and sequential DNA-RNA FISH could identify the Xi in some nuclei (Figure S1E). We classified the Xist/XIST RNA FISH localization patterns into four groups, as done previously for lymphocytes: type I nuclei have the canonical robust Xist RNA "clouds"; type II nuclei exhibit diffuse Xist RNA signals within a nuclear area encompassing the X chromosome; type III nuclei have dispersed pinpoints of Xist RNA across the nucleus; type IV nuclei lack

Figure 1. Xist RNA is not robustly localized at the Xi in mouse and human AT2 cells

(A) Representative field images of Xist RNA FISH in female mouse AT2 cells isolated from lung. Scale bar is 10 micron.

(B) Representative field images of XIST RNA FISH in human female AT2 cells. Scale bar is 10 micron.

(C) Cartoon showing each category of Xist RNA localization pattern observed in AT2 cells.

(D and E) Quantification of XIST RNA localization patterns for (D) mouse AT2 cells and (E) human AT2 cells. Number of nuclei counted is above each column. Statistical significance determined using t test with unequal variance comparing AT2 with fibroblasts for each category of Xist localization pattern (types I, II, III, IV).

(F) qRT-PCR for *Xist* expression in mouse AT2 cells, transformed female MEFs (with multiple X chromosomes), and primary B cells from female mice. Error bars denote standard error of mean.

(G) qRT-PCR for *XIST* expression in human AT2 cells and primary female fibroblasts (IMR-90). Error bars denote standard error of mean.

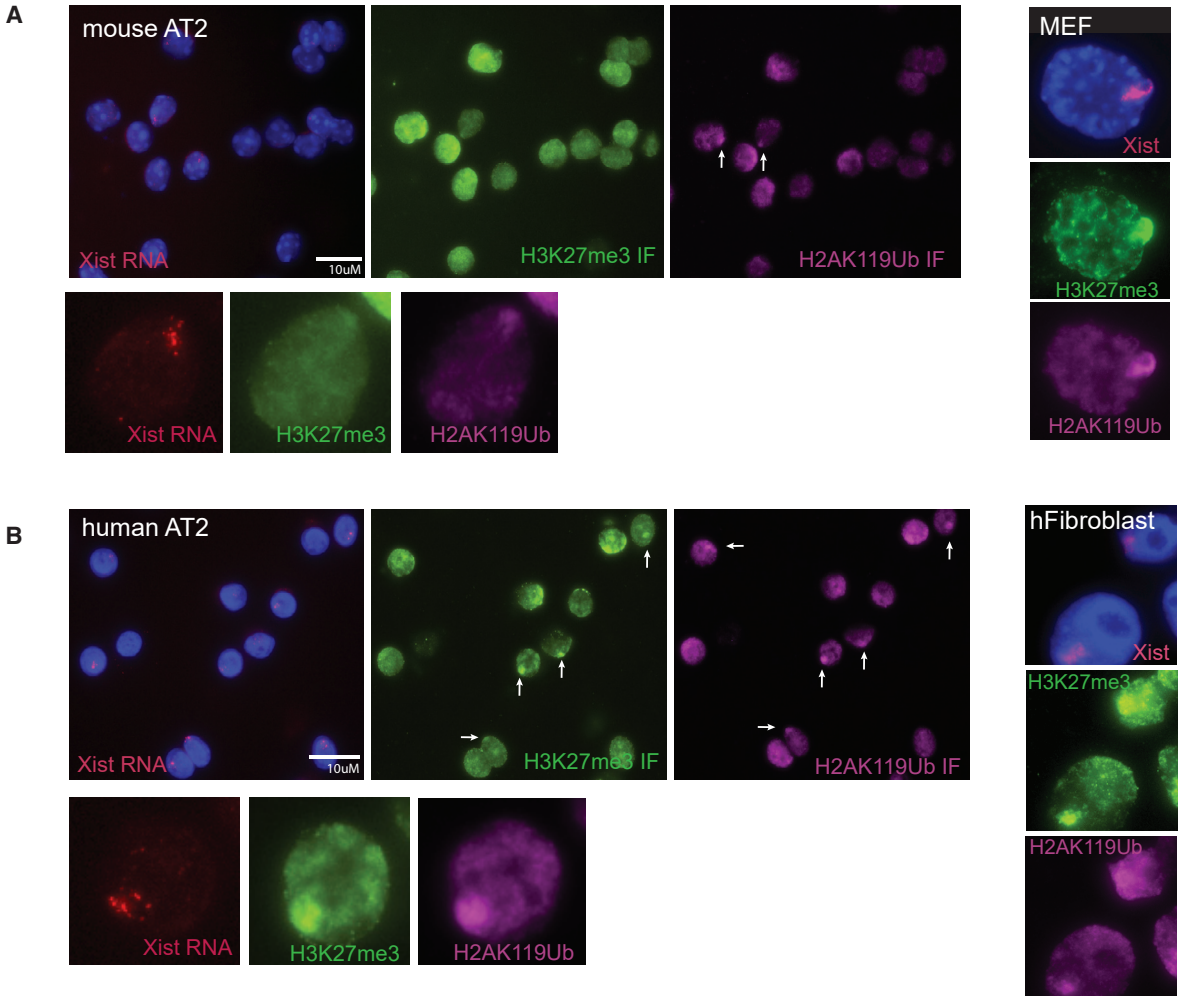

(legend on next page)

Xist RNA signals (Figure 1C) (Pyfrom et al., 2021; Syrett et al., 2019; Wang et al., 2016). We found that Xist RNA patterns in mouse AT2s were predominantly types III and IV, and had significantly fewer type I and II patterns compared with MEFs (Figure 1D). Interestingly, human AT2 cells had more detectable XIST RNA transcripts than mouse AT2s, and consisted of mostly type II and type III patterns (Figure 1E). Human AT2 cells, similar to mouse AT2s, also had significantly fewer type I patterns compared with human fibroblasts. *Xist* was abundantly expressed in both mouse and human AT2 cells, at similar levels to primary mouse B cells and also fibroblasts (Figures 1F and 1G). Taken together, female AT2 cells from both mouse and human lack robust Xist/XIST RNA localization at the Xi.

The Xi in female AT2 cells has reduced levels of heterochromatic foci

In most somatic cells, the Xi is enriched for heterochromatic modifications that can be visualized cytologically by immunofluorescence (IF) (Payer and Lee, 2008; Plath et al., 2003). Because AT2 cells lacked robust Xist/XIST RNA clouds, we next performed sequential Xist RNA FISH and IF for two histone modifications, H3K27me3 and H2AK119-ubiquitin (Ub), typically associated with XCI. Mouse AT2 cells had low levels of detectable foci of H3K27me3 and H2AK119Ub (white arrows in Figure 2A), and foci were present in cells that had more Xist RNA signals (type II). Human AT2 cells had more H3K27me3 and H2AK119Ub foci compared with mouse cells (white arrows in Figure 2B), and IF foci were present in cells with type II XIST RNA. We quantified the number of nuclei with co-localization of Xist RNA and IF focus, nuclei containing just an IF focus, nuclei with just Xist RNA signal, and nuclei lacking both Xist RNA and IF focus, for both mouse and human AT2 cells. We found that less than 5% of mouse AT2 nuclei exhibited co-localization of Xist RNA and heterochromatic focus (H3K27me3 or H2AK119Ub), and about 15%–20% of nuclei contained a focus of either mark (Figure 2C). The majority of mouse AT2 nuclei lacked IF foci and Xist RNA signals. Human AT2 cells had higher percentages of nuclei with co-localization of XIST RNA and a heterochromatic focus (blue bars; 5%–25%) (Figure 2D), in keeping with human AT2s exhibiting more detectable Xist RNA patterns. Similar to mouse cells, human AT2s exhibited 5%–15% of nuclei with a heterochromatic focus. Fibroblasts from mouse and human samples contained high levels of co-localization of Xist/XIST RNA signal with heterochromatic foci. In sum, the Xi in mouse and human AT2 cells has reduced enrichment of two heterochromatic histone modifications, H3K27me3 and H2AK119Ub, a finding more prominent in mouse than in human cells.

Over half of the expressed X-linked genes escape XCI in female AT2 cells, including *Ace2*

The atypical localization of Xist RNA and heterochromatic modifications H3K27me3 and H2AK119Ub at the Xi in AT2 cells suggests that there could be increased transcription from the Xi. XCI silences most genes across the X in female cells, but there are genes that "escape" XCI and are transcribed from both the Xi and active X chromosome (Xa) (Berletch et al., 2010, 2015). About 3%–7% of the mouse X chromosome escapes XCI in brain, ovary, and splenic tissues (Berletch et al., 2015), and human tissues exhibit much higher levels of XCI escape that ranges from 25% to 35% (Tukiainen et al., 2017). To determine the allele-specific expression of X-linked genes in mouse AT2 cells, we mated C57BL/6 females heterozygous for a deletion of exons 1–3 of Xist (Csankovszki et al., 1999) ($X^{Xist\ KO}\ X^{wt}$) to *Mus castaneus* (*cast*) male mice to generate F1 mus/cast progeny where female mice ($Xa^{Xist\ KO}\ Xi^{cast}$) have completely skewed XCI across all tissues, as all Xi are derived from the *cast* allele, which can be distinguished from the Xa (C57BL/6) allele by multiple SNPs (Figure 3A). We isolated AT2 cells from four female F1 mus/cast mice for RNA sequencing (RNA-seq) to determine allele-specific reads based on SNPs. We also isolated AT2 cells from four male F1 mus/cast mice for RNA-seq to determine sex-specific gene expression profiles, confirming extremely high sort purity in all samples (Figures S1A–S1C).

Figure 2. Heterochromatic modifications H3K27me3 and H2AK119-ubiquitin (Ub) are not enriched at the Xi in mouse and human AT2 cells

(A) Sequential Xist RNA FISH followed by IF detection for H3K27me3 (FITC) and H2AK119Ub (Cy5) for mouse AT2 cells; a representative field image (same left to right) is shown. Zoomed-in images for a representative nucleus are shown below the field images. White arrows denote IF foci. Control IF staining using MEFs is shown. Scale bar is 10 micron.

(B) Sequential Xist RNA FISH followed by IF detection for H3K27me3 (FITC) and H2AK119Ub (Cy5) for human AT2 cells; representative field image is shown. Zoomed-in images for a representative nucleus are shown below the field images. White arrows denote IF foci. Control IF staining using human fibroblasts (293T) is shown. Scale bar is 10 micron.

(C) Quantification of Xist RNA and IF co-localization patterns for AT2 cells isolated from three distinct female mice (m3, m4, m5) and MEFs from n = 2 female mice.

(D) Quantification of Xist RNA and IF co-localization patterns for AT2 cells isolated from three distinct healthy human donors (HD1, HD2, HD3) and 293T cells (two replicate experiments). Number of nuclei counted is above each column.

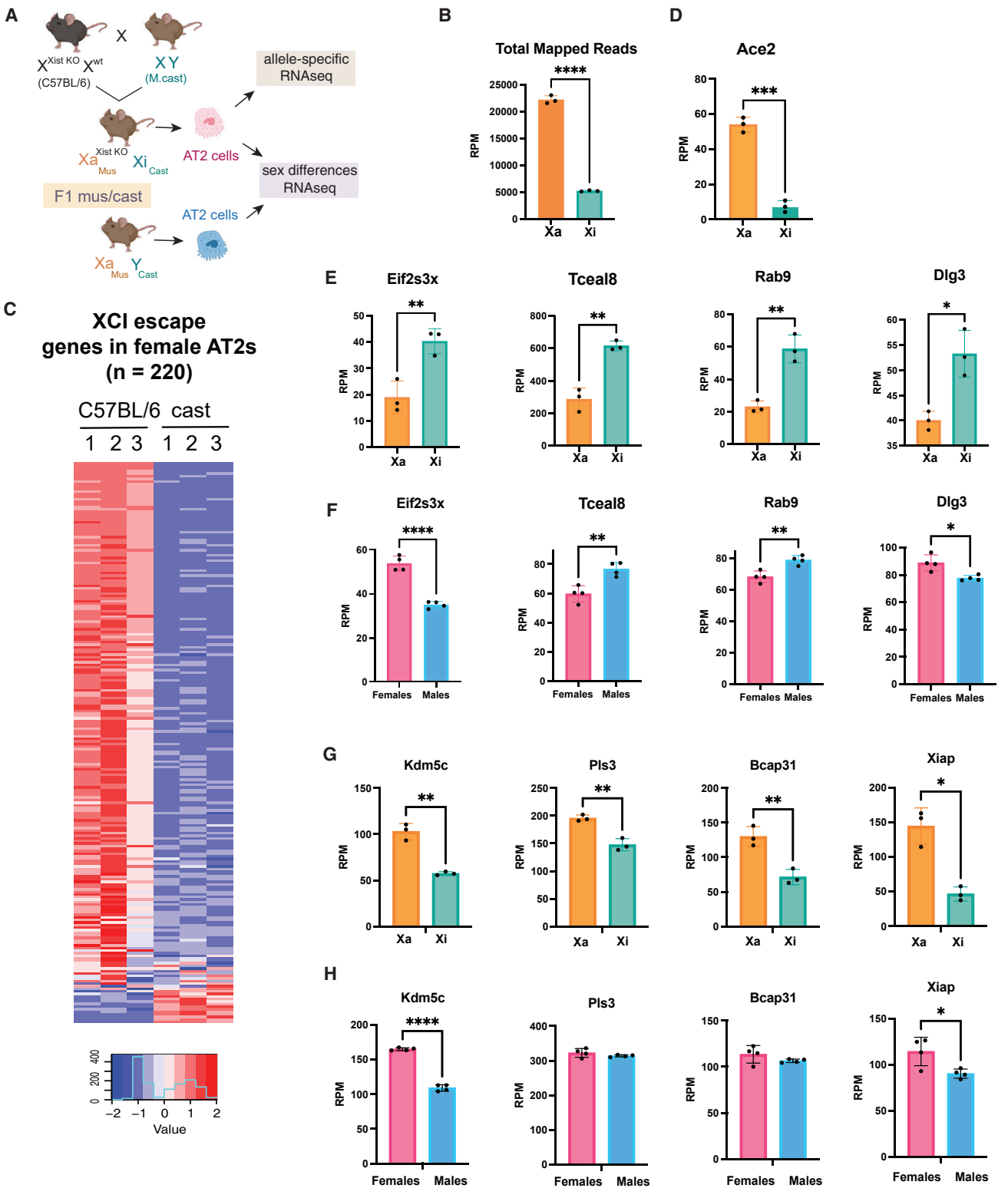

(legend on next page)

To determine the reads that mapped to each parental genome, we separately aligned RNA-seq reads to the C57BL/6 and *castaneus EiJ* genomes. Reads that did not map were then aligned to the other genome to generate uniquely mapped reads in two categories: (1) C57BL/6 reads that contain C57BL/6 specific SNPs; and (2) *castaneus* reads that contain specific *castaneus* SNPs (Figure S1F). We calculated diploid gene expression for all mapped reads to determine reads per million (RPM), and defined the SNP-based haploid gene expression for Xi (Xi-SRPM) or Xa (Xa-SRPM) to be allele-specific SNP-containing exonic reads per 10 million uniquely mapped reads (Berletch et al., 2015). To validate our allele-specific mapping, we examined autosomal imprinted gene expression in female and male AT2 cell samples (Figures S2A and S2B). *Meg3* is a maternally expressed gene and was expressed exclusively from the maternal C57BL/6 allele in both male and female AT2 cells (Figure S2A). *Peg3* is paternally expressed and was predominantly expressed from the cast allele in both male and female samples (Figure S2B). We also validated that reads from the *Xist/Tsix* region were predominantly expressed from the *cast* allele in female AT2 cells, and detected some expression (~40 RPM) from Xa in this region (Figures S2C and S2D). The allelic distribution of mapped reads across autosomal chromosomes was similar for C57BL/6 and *cast* alleles and the geometric mean of ratios was nearly equal to 1, yet we observed a significant skew for allelic X-linked gene expression in AT2 cells (Figure S2E). We observed significantly higher reads that mapped to the Xa compared with the Xi, yet we also found that about 25% of total X-linked mapped reads were expressed from the Xi, unlike the total mapped reads for chromosome 1, which were similar for both alleles (Figure S2F). Indeed, the geometric mean of ratios for autosomal allelic expression were similar for C57BL/6 and cast reads, yet we observed an expected X-linked skew for Xa reads (C57BL/6) relative to Xi reads (cast) (Figure S2G). Taken together, while the Xi in female AT2 cells is still dosage compensated, there is a very significant amount of transcription specifically from the Xi.

For female F1 mus/cast samples (n = 3), we used a published binomial model to identify escape genes and estimated a statistical confidence of escape probability (Berletch et al., 2015). We found that there are 465 X-linked genes with detectable expression in AT2 cells (RPM >1), and 455 of these genes are expressed in both male and female AT2 cells (Figure S3A). Approximately 327 X-linked genes are expressed allele-specifically (with detectable SNPs) in female AT2 cells (Figure S3B). Using the binomial model to identify XCI escape genes in AT2s, we determined that 223 (68%) genes escape XCI at a 99% confidence with a p-value cutoff of 0.01 (Figure 3C and Table S1). The majority of AT2 XCI escape genes are novel, and just nine of these genes have been previously reported to escape XCI in mouse brain, ovary, and spleen tissue (Berletch et al., 2015). We also found that *Ace2* escapes XCI in AT2 cells (Figure 3D) and has higher expression in AT2 cells compared with fibroblasts (Figure S3C). XCI escape genes were distributed across the X and did not cluster in specific regions (Figure S3D), perhaps reflecting the paucity of Xist RNA and heterochromatic modifications across the Xi (Figures 1 and 2). Surprisingly, we observed ~20 X-linked genes which have higher expression from the Xi compared with the Xi (Figures 3C and S3B; Table S1). Some XCI escape genes with Xi/Xa ratios >1 include *Gla*, *Bex1*, *Pin4*, *Eif2s3x*, *Tceal8*, *Rab 9*, *Dlg3*, and *Xist* (Figure 3E and Table S1). We observed that XCI escape genes with Xi/Xa ratios >1 were expressed in a sex-biased fashion, but the direction of the bias varied (Figure 3F). For example, *Eif2s3x* was expressed at higher levels in female AT2 cells whereas *Tceal8* exhibited higher expression in male AT2 cells (Figure 3F). The majority of XCI escape genes expressed in female

Figure 3. Female AT2 cells have over 200 X-linked genes that escape XCI

(A) Schematic diagram showing mouse mating strategy to generate F1 mus/cast female mice with skewed XCI. In these mice, the maternal X (C57BL/6) carries the Xist deletion and is the active X (Xa), and the paternal X is always inactivated (Xi) and expresses *Xist*. We also isolated AT2 cells from male F1 mus/cast mice to determine sex-specific gene expression profiling.

(B) Allelic specific reads (RPM) for each expressed X-linked gene which map to the Xa (orange) or Xi (teal). Error bars are standard error of the mean.

(C) Heatmap showing the allele-specific expression for XCI escape genes in AT2 cells. Each replicate sample (1–3) is shown for reads derived from the C57BL/6 or cast allele.

(D) *Ace2* is an XCI escape gene in AT2 cells.

(E) Normalized haploid mapped reads from the Xa (orange) and Xi (teal) for four XCI escape genes where there is more expression from the Xi compared with the Xa (Xi > Xa). Error bars are standard error of the mean.

(F) Normalized diploid mapped reads from female (pink) and male (blue) AT2 samples for four XCI escape genes with Xi > Xa. Error bars are standard error of the mean.

(G) Normalized haploid mapped reads from the Xa (orange) and Xi (teal) for the top three XCI escape genes with the highest expression in female AT2 cells. Error bars are standard error of the mean.

(H) Normalized diploid mapped reads from female (pink) and male (blue) samples for the top three XCI escape genes. Statistical significance determined using unpaired t tests for panels B–H (excluding C). Error bars are standard error of the mean.

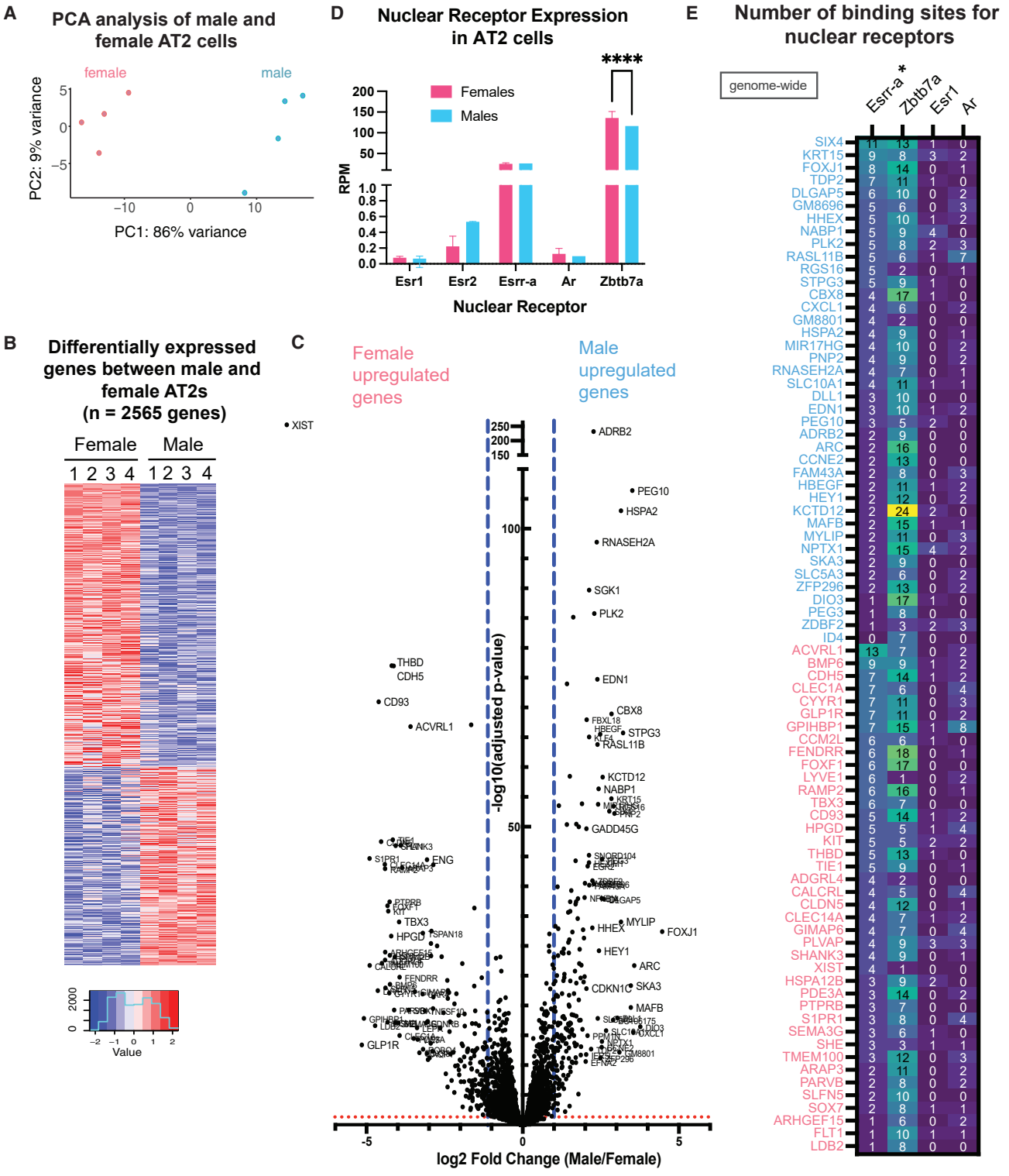

Figure 4. AT2 cells exhibit sex-biased expression of autosomal and sex chromosome genes

(A) Principal component analyses (PCA) for the four replicate male (blue) and female (pink) AT2 samples.

(B) Heatmap showing DEGs (a total of 2,565 genes) between replicate male and female AT2 samples.

(legend continued on next page)

AT2 cells had higher expression from the Xa (Figure 3G; complete list in Table S1), and some also exhibited sex-biased expression (Figure 3H), suggesting that expression of many escape genes may be otherwise compensated at the transcriptional level to normalize expression between sexes. Gene ontology (GO) analysis for the 223 XCI escape genes revealed significant enrichment of pathways for regulation of dosage compensation, nucleotide metabolism, chromatin organization, and regulation of cellular component organization (Table S3C). Thus 68% of all X-linked genes expressed in female AT2 cells escape XCI, and some of these X-linked genes exhibit significant sex-biased expression.

Next we examined allelic expression for autosomal genes that are typical markers for AT2 cells. In keeping with their homeostatic physiological function as the primary producer of pulmonary surfactant, we found that the surfactant protein gene *Sftpc* was expressed at significantly higher levels from the maternal allele compared with the paternal allele (Figures S3E and S3F) in both male and female AT2s (Figure S3G). We also observed that *Lamp3*, *Muc1*, and *Abac3* exhibited allelic differences in expression in female AT2s (Figure S3F). However, these allelic expression differences did not significantly impact overall expression on comparing female with male samples (Figure S3G).

Sex-biased gene expression is a prominent feature of mouse AT2s

We compared the global gene expression profiles in male and female AT2s using principal component analysis (PCA) for both autosomal and sex-linked genes. We observed that female AT2 samples grouped apart from male samples in the PC1 component (with 86% variance; Figure 4A). Indeed, we found that there were 2,565 genes that were differentially expressed between male and female AT2s (RPM in all four female samples >1; adjusted $p < 0.05$ across all four replicates; Figures 4B and 4C). The majority of the differentially expressed genes (DEGs) were autosomal, yet we observed some X-linked genes that were significantly overexpressed greater than $\log_2$ fold change in male AT2s (*GM6568*, *Rbm3*, *Rtl5*, *Zfp711*) and female AT2s (*Tspan7*, *Tex11*, *Slc25A43*, *Mtcp1*) (Figure S4A). While the relatively high number of DEGs was somewhat surprising, we note that only 510 genes show greater than 2.0 fold change between male and females, highlighting genes whose expression differences are most likely to result in phenotypic manifestations. We found that the β2-adrenergic receptor (*Adrb2*) was the most upregulated gene in male AT2 cells, along with various imprinted genes including *Peg10* and *Gnas* (Figure S4B), which is part of the G-protein-coupled receptor-regulated adenylyl cyclase signal transduction pathway downstream of Adrb2. As expected, *Xist* was the most significantly upregulated gene in female AT2 cells (Figures 4C and S4A). GO analyses revealed that the female-specific enrichment included pathways of autophagy, protein modification, catabolic processes, and phosphatidylinositol biosynthetic processes (Figure S4C and Table S3A). The top five pathways enriched in male samples included nonsense-mediated decay, mRNA processing, Parkinson's disease, cholesterol biosynthesis, and nucleobase-containing biosynthetic pathways (Figure S4C and Table S3B). While we did observe some differential expression of genes typically not associated with the AT2 lineage (e.g., *Foxj1*), equivalent expression of essentially all major AT2 marker genes strongly indicates that these unexpected expression differences are biologically valid.

Because of the large number of sex-specific DEGs, we asked whether AT2 cells exhibited expression differences in hormone or nuclear receptor transcription factors and whether genes expressed in AT2 cells were enriched for hormone receptor binding sites. We examined the expression levels for known hormone and nuclear receptors in male and female AT2s and found that the nuclear orphan receptor *Esrr-α* and transcription factor *Zbtb7a*, which mediates AR activity, were significantly expressed at RPM values greater than 1, unlike estrogen receptors *Esr1* and *Esr2*, and the androgen receptor *Ar* (Figure 4D). We found a significant difference in expression of *Zbtb7a* between male and female AT2s, yet expression levels for *Esrr-α* were similar for both sexes. Next, we determined the number of binding sites for hormone (Esr1, Ar) and nuclear receptors (Esrr-α, Zbtb7a) present within 2 kb of the transcriptional start site (TSS) for the top 40 DEGs (genome-wide) in male and female AT2s (Figure 4E). We found that there were more nuclear receptor binding sites (Esrr-α, Zbtb7a) compared with hormone receptor sites (Esr1, Ar) present in these genes, which exhibited sex-biased expression in AT2s. Comparing binding sites between male and female DEGs, we found that Esrr-α sites were significantly higher ($p = 0.048$) in male upregulated DEGs, yet the number of binding sites for Zbtb7a, Esr1, and Ar were similar for

(C) Volcano plot of female upregulated genes (left) and male upregulated genes (right) expressed in AT2 cells. Blue dashed lines indicate the cutoff for $\log_2$ fold change of expression (x axis), and the y axis is the adjusted p value for significance of differential expression.
(D) Normalized diploid mapped reads for male (blue) and female (pink) AT2 samples of nuclear receptor transcription factors. Statistical significance determined using Student's unpaired t test. Error bars are standard error of the mean.
(E) Numbers of binding sites for hormone (Ar, Esr1) and nuclear receptor (Esrr-α and Zbtb7a) transcription factors in promoter regions (2 kb of TSS) of the top 40 DEGs (genome-wide) upregulated in male (blue) or female (pink) AT2 cells.

both male and female upregulated genes (Figure 4E). Next, we determined the hormone and nuclear receptor binding sites for the XCI escape genes expressed in AT2 cells. We observed that there were higher numbers of nuclear receptor binding sites compared with hormone receptor sites for XCI escape genes (Figure S4D). There were similar numbers of Esrr-α and Zbtb7a binding sites across XCI escape genes, irrespective of whether there was more (top) or less (bottom) expression from the Xi (Figure S4D). This suggests that differential binding of these nuclear receptors may not account for the differences in expression between the two groups of XCI escape genes. One exception could be the XCI escape gene *Gla*, which has the most Esr1 binding sites in this list and exhibits higher expression from the Xi compared with the Xa. We observed some Ar binding sites across both groups of XCI escape genes, which suggests that Ar could increase transcription from some genes on the Xa in male cells. In conclusion, while AT2 cells have low expression of the estrogen receptors (*Esr1*, *Esr2*) and the androgen receptor (*Ar*), there is higher expression of the nuclear orphan receptor *Esrr-α* and transcription factor *Zbtb7a*, which may influence sex-biased expression genome-wide.

DISCUSSION

The prevailing model of XCI maintenance indicates that all somatic cells utilize the same epigenetic mechanisms to maintain transcriptional silencing of the Xi for dosage compensation of X-linked genes between males and females. Here we show that female AT2 cells from mouse and human lung contain an Xi that lacks canonical enrichment of Xist RNA and heterochromatic modifications H3K27me3 and H2AK119Ub, suggesting that there could be more expression or "XCI escape" in this cell type. Our studies demonstrate that AT2 cells have the highest levels of XCI escape for mouse cells reported to date, where approximately 68% of expressed X-linked genes are transcribed from the Xi and Xa, and XCI escape genes are distributed across the Xi chromosome. We propose that the reductions with Xist RNA, H3K27me3, and H2AK119Ub enrichment contribute toward increased XCI escape across the Xi in AT2 cells. Our experiments demonstrate that AT2 cells, similar to immune cells (Pyfrom et al., 2021; Syrett et al., 2018, 2019; Wang et al., 2016), do not strictly follow the canonical "rules" of XCI maintenance, which likely reflects a necessity for specific increased expression from the Xi for biological functions.

One surprising discovery is that about 20 XCI escape genes exhibited higher expression from the Xi compared with the Xa in AT2 cells, which is another unique feature of XCI maintenance specific to these cells. XCI escape genes are typically expressed at lower levels from the Xi compared with expression from the Xa (Berletch et al., 2010, 2015). We predicted that increased Xi expression would perhaps result in higher female expression for these genes; however, we observed that the sex-biased expression did not follow a trend that consistently favored either male or female. Our results are in agreement with previous work suggesting that XCI escape is a significant source of sex-biased expression (Balaton and Brown, 2016; Johnston et al., 2008; Tukiainen et al., 2017), although in this study we did not observe consistently higher female expression for XCI escape genes. Possible mechanisms that might contribute toward allele-specific expression differences of XCI escape genes could involve epigenetic modification enrichment differences between the X chromosomes (such as DNA methylation or histone modifications) or transcription factors that would preferentially activate one allele more than the other. Our observation that XCI escape genes expressed in AT2 cells exhibited high numbers of Esrr-α binding sites makes it intriguing to consider that there may be differential binding of the Esrr-α receptor and co-activator (or co-repressor) proteins that results in allelic expression differences.

The SARS-CoV-2 receptor, *Ace2*, is located on the X chromosome, and an important unanswered question has been whether this gene escapes XCI in cell types important in COVID-19. Previous work using hybrid fibroblast cell lines indicated that *ACE2* exhibits variable escape (Balaton et al., 2015; Tukiainen et al., 2017); however, some of these cells are immortalized and thus do not reflect a physiological context. We hypothesized that if *ACE2* escaped XCI in AT2 cells, women might produce more ACE2 protein and be subject to higher viral infection/titers yet also might exhibit enhanced lung repair compared with men. Even though *Ace2* is biallelically expressed in mouse AT2s, we did not observe sex differences in the steady-state levels of Ace2 mRNA, although there still could be differences in Ace2 protein levels in these cells. Our studies demonstrate that *Ace2* is an XCI escape gene in mouse AT2 cells and may also likely escape XCI in human AT2 cells. We were unable to detect biallelic expression of *ACE2* in human AT2 cells because of poor signal resolution using RNA FISH (data not shown), so it remains an open question whether *ACE2* escapes XCI in human AT2 cells. However, because there are significantly higher numbers of XCI escape genes in human cells compared with mouse (Berletch et al., 2010, 2011), it is very likely that *ACE2* would also escape XCI in human AT2s. While *Ace2* escapes XCI in AT2 cells, we found that there are similar levels of *Ace2* expression in male and female AT2s. This result could be explained by observations that XCI escape genes sometimes, but not always, contribute toward sex-biased expression (Tukiainen et al., 2017).

While fetal lungs and fetal lung epithelial cells have been shown to exhibit some sex-specific differences in cell number, gene expression, and cellular function (Kaltofen et al., 2015; McCoy et al., 1999; Simard et al., 2006), this study is the first to directly assess genome-wide transcriptional differences between male and female adult AT2s. Over 2,500 genes exhibited significant sex-related differences of expression in mouse AT2 cells. Our findings suggest that these expression differences may underlie the observed sex differences in pulmonary disease prevalence and severity. Human males are at higher risk for severe COVID-19 disease (Scully et al., 2020; Takahashi et al., 2020), and males also experience greater prevalence and severity of interstitial lung disease and pulmonary fibrosis (Kawano-Dourado et al., 2021). Intriguingly, these pathologies are increasingly recognized as being driven by defects in the lung epithelium, primarily AT2 cells (Camelo et al., 2014; Katzen and Beers, 2020; Parimon et al., 2020), reinforcing the relevance of the AT2 transcriptomic differences between the sexes. However, females are more likely to develop ARDS after traumatic injury (Heffernan et al., 2011), and once ARDS has developed women are at higher risk of death (McNicholas et al., 2019), which may reflect the fact that females have stronger immune responses compared with males (Fischer et al., 2015; Klein and Flanagan, 2016). How biallelic ACE2 expression, and whether there are sex differences in ACE2 protein levels in AT2 cells, contributes to ARDS-induced disease warrants further investigation.

The underlying drivers of the sex-specific transcriptional differences observed here are almost certainly multifactorial. We found that some genes exhibiting greater expression in females also demonstrate escape from XCI, and that there are many DEGs genome-wide. Likely candidates for these sex-biased gene signatures include hormone receptors, which are expressed at low levels (below 1 RPM) in AT2 cells. However, we cannot exclude the possibility that these proteins are present, albeit at low concentrations, in AT2 cells, and likely influence gene expression. We found that there are both Esr1 and Ar binding sites in nearly all of the top 40 male and female DEGs (Figure 4E). The DEGs contained higher numbers of Esrr-α and Zbtb7a binding sites compared with Esr1 and Ar across both male and female upregulated DEGs. While we did not detect significant gene expression differences for *Esrr-α*, we found that that there were significantly fewer *Zbtb7a* reads in male AT2 samples (Figure 4D), which might result in less Zbtb7a protein and transcriptional repression, contributing to increased expression of male upregulated DEGs (Figure 4E, genes in blue).

In summary, our studies have revealed unexpected differences in XCI maintenance in both mouse and human AT2s, and we propose that reduced Xist RNA and heterochromatic histone modifications could contribute to the high levels of XCI escape across the Xi in mouse AT2 cells. Additionally, we observed a surprisingly large number of genes exhibiting sex-specific expression, which suggests that there could be both genetic and epigenetic contributions for sex biases in lung injury and repair, including both acute (ARDS) and progressive (interstitial lung) disease. Our work is an important first step for understanding the role of sex in lung injury and chronic pathology, and could ultimately contribute to the design of novel sex-specific therapeutic approaches to improve lung repair.

EXPERIMENTAL PROCEDURES

Resource availability

Corresponding author

Further information and requests for resources and reagents should be directed to and will be fulfilled by the corresponding author, Montserrat C. Anguera (anguera@vet.upenn.edu).

Materials availability

This study did not generate new unique reagents.

Data and code availability

The RNA-seq data are available in the Gene Expression Omnibus database under accession GEO: GSE203166.

AT2 cell isolation

Lungs were inflated with 5 U/mL dispase II in Hanks' balanced salt solution (Thermo Fisher Scientific), tying off the trachea and cutting lobes away from the main stem bronchi. Lungs were incubated in dispase for 45 min shaking at room temperature, and mechanically dissociated by pipetting in sort buffer (SB; Dulbecco's modified Eagle's medium [DMEM; Thermo Fisher] + 2% cosmic calf serum [CC; Thermo Fisher] + 1% penicillin/streptomycin [P/S]). After pelleting at 550 × *g* for 5 min at 4°C, the whole-lung suspension was treated with Red Blood Cell Lysis buffer (Millipore Sigma) for 5 min, pelleted, and resuspended in SB + 1:1,000 DNase I (Millipore Sigma) for a 45-min recovery period while shaking at 37°C. Whole-lung suspension was then resuspended in SB + 1:50 TruStain FcX (anti-mouse CD16/32) antibody (BioLegend) for a 10-min blocking period at 37°C. For sorts from *C57BL6* mice, AT2 cells were collected using allophycocyanin (APC)/Cy7-conjugated rat anti-mouse CD45 antibody (1:200; BioLegend, 30-F11), Alexa Fluor 488-conjugated rat anti-mouse CD326 (EpCAM) antibody (1:200; BioLegend, G8.8), and phycoerythrin (PE)-conjugated rat anti-mouse CD104 (integrin β4) antibody (1:100; BioLegend, 346-11A). Staining was performed for 45 min at 4°C, followed by a final spin-down at 550 × *g* for 5 min at 4°C. Stained cells and fluorescence-minus-one controls were then resuspended in SB + 1:1,000 DNase + 1:1,000 Draq7 (Beckman Coulter) as a live/dead stain. All fluorescence-activated cell sorting (FACS) was done on a BD FACS Aria Fusion (BD Biosciences), and cells were collected in Falcon round-bottom polystyrene tubes (Thermo Fisher) in 300 μL of DMEM + 20% CC + 2% P/S. Purity of sorted AT2s was routinely performed for each sample as demonstrated in Figure S1.

RNA FISH

For Xist RNA FISH, AT2 cells (mouse and human) were immediately cytospun onto glass slides after FACS, then incubated in ice-cold cytoskeletal (CSK) buffer containing 0.5% Triton X-100 for 3 min, fixed in 4% paraformaldehyde for 10 min, and dehydrated using an ethanol series. For Xist RNA FISH we used two Cy3-labeled oligonucleotide probes, which target repetitive regions within *Xist* exon 1 (Wang et al., 2016). Images were obtained using a Nikon Eclipse microscope and were categorized by the type of Xist RNA localization patterns as shown in Figure 1C and as described previously (Syrett et al., 2017, 2018; Wang et al., 2016).

XCI gene escape from allele-specific RNA sequencing

Genes that escape XCI were identified using three thresholds of escape, as previously described (Berletch et al., 2015). In brief, diploid gene expression was first calculated in RPKM (reads per kilobase of exon length per million mapped reads), and genes were called expressed if their diploid RPKM was >1. For every X-linked gene that passed this threshold, haploid gene expression was calculated in SRPM, and genes which had an Xi-SRPM >2 were considered to be expressed from the Xi. Finally, a binomial model estimating the statistical confidence of escape probability was applied to the genes passing the first two thresholds. This model compares the proportion of Xi-specific reads with the total X-linked reads (Xi + Xa) and calculates a 95% confidence interval. If the 95% lower confidence limit of a gene's escape probability was greater than 0, it was called an escape gene.

RNA-seq methods

Using the same fastq files generated for the allele-specific alignment, a separate pipeline was used to quantify standard, diploid gene expression. Reads were aligned to the mm10 genome build using the ultrafast STAR aligner (Dobin et al., 2013) with default parameters and "—quantmode GeneCounts" to quantify gene expression. Read counts generated by STAR were used as input for the DeSeq2 R package to identify DEGs between male and female samples. RPM were also calculated, and a gene was considered expressed if it had an RPM >1 in all female samples. GO analyses were determined using the Metascape platform (Zhou et al., 2019). RNA-seq data are available in the GEO database under accession GEO: GSE203166.

SUPPLEMENTAL INFORMATION

Supplemental information can be found online at https://doi.org/10.1016/j.stemcr.2022.12.005.

AUTHOR CONTRIBUTIONS

M.C.A. and A.E.V. wrote and edited the manuscript. M.C.A. made the figures from data collected and generated by I.S. and S.P. The AT2 cells were isolated by A.W., G.Z., and A.E.V. The Xist/XIST RNA FISH and IF of human and mouse AT2 cells was performed by I.S. All bioinformatic analyses were performed by S.P. The allele-specific RNA-seq pipeline was developed by X.Y. while training in the lab of B.D.G. A.D. performed genotyping, F1 mus × cast mice organization, and mouse preparation for sorting.

ACKNOWLEDGMENTS

We would like to thank L. King for assistance with editing of the manuscript; Z. Beethem for modifications to the code for calculating the confidence intervals for XCI escape genes; D. Beiting of PennVet CHMI for RNA-seq library preparation; N. Jiwrajka for imaging assistance; and all members of the Anguera and Vaughan labs for helpful discussions. We also greatly appreciate the efforts of L. Carrel, H. Markus, and D. Liu for RNA-seq analyses of hAT2 cells. We also thank BioRender for using some of their stock images for figures in this paper. This research was supported by an Administrative Supplement to NIH R01 AI134834 (to M.C.A.), NIH R21 AI164006 (to M.C.A.), Penn IRM COVID pilot grant (to M.C.A. and A.E.V.), Penn Vet COVID/CHMI pilot grant (to M.C.A. and A.E.V.), Lupus Research Foundation Insight award (to M.C.A.), NIH 1F31GM136073-01 to I.S., NIH 1F32AI154797-01 to S.P., and NIH R01HL153539 and Lisa Dean Moseley Research grant to A.V.

CONFLICT OF INTERESTS

The authors declare no competing interests.

Received: May 24, 2022
Revised: December 7, 2022
Accepted: December 8, 2022
Published: January 12, 2023

REFERENCES

Anguera, M.C., Sadreyev, R., Zhang, Z., Szanto, A., Payer, B., Sheridan, S.D., Kwok, S., Haggarty, S.J., Sur, M., Alvarez, J., et al. (2012). Molecular signatures of human induced pluripotent stem cells highlight sex differences and cancer genes. Cell Stem Cell *11*, 75–90. https://doi.org/10.1016/j.stem.2012.03.008.

Balaton, B.P., and Brown, C.J. (2016). Escape artists of the X chromosome. Trends Genet. *32*, 348–359. https://doi.org/10.1016/j.tig.2016.03.007.

Balaton, B.P., Cotton, A.M., and Brown, C.J. (2015). Derivation of consensus inactivation status for X-linked genes from genome-wide studies. Biol. Sex Differ. *6*, 35. https://doi.org/10.1186/s13293-015-0053-7.

Barkauskas, C.E., Cronce, M.J., Rackley, C.R., Bowie, E.J., Keene, D.R., Stripp, B.R., Randell, S.H., Noble, P.W., and Hogan, B.L.M. (2013). Type 2 alveolar cells are stem cells in adult lung. J. Clin. Invest. *123*, 3025–3036. https://doi.org/10.1172/JCI68782.

Berletch, J.B., Yang, F., and Disteche, C.M. (2010). Escape from X inactivation in mice and humans. Genome Biol. *11*, 213. https://doi.org/10.1186/gb-2010-11-6-213.

Berletch, J.B., Yang, F., Xu, J., Carrel, L., and Disteche, C.M. (2011). Genes that escape from X inactivation. Hum. Genet. *130*, 237–245. https://doi.org/10.1007/s00439-011-1011-z.

Berletch, J.B., Ma, W., Yang, F., Shendure, J., Noble, W.S., Disteche, C.M., and Deng, X. (2015). Escape from X inactivation varies in mouse tissues. PLoS Genet. *11*, e1005079. https://doi.org/10.1371/journal.pgen.1005079.

Camelo, A., Dunmore, R., Sleeman, M.A., and Clarke, D.L. (2014). The epithelium in idiopathic pulmonary fibrosis: breaking the barrier. Front. Pharmacol. *4*, 173. https://doi.org/10.3389/fphar.2013.00173.

CDC COVID-19 Response Team (2020). Severe outcomes among patients with coronavirus disease 2019 (COVID-19) — United States, February 12–March 16, 2020. MMWR Morb. Mortal. Wkly. Rep. *69*, 343–346.

Channappanavar, R., Fett, C., Mack, M., Ten Eyck, P.P., Meyerholz, D.K., and Perlman, S. (2017). Sex-based differences in susceptibility to severe acute respiratory syndrome coronavirus infection. J. Immunol. *198*, 4046–4053. https://doi.org/10.4049/jimmunol.1601896.

Chapman, H.A., Li, X., Alexander, J.P., Brumwell, A., Lorizio, W., Tan, K., Sonnenberg, A., Wei, Y., and Vu, T.H. (2011). Integrin alpha6beta4 identifies an adult distal lung epithelial population with regenerative potential in mice. J. Clin. Invest. *121*, 2855–2862. https://doi.org/10.1172/JCI57673.

Chen, J., Jiang, Q., Xia, X., Liu, K., Yu, Z., Tao, W., Gong, W., and Han, J.J. (2020). Individual variation of the SARS-CoV2 receptor ACE2 gene expression and regulation. Aging Cell *19*, e13168.

Csankovszki, G., Panning, B., Bates, B., Pehrson, J.R., and Jaenisch, R. (1999). Conditional deletion of Xist disrupts histone macroH2A localization but not maintenance of X inactivation. Nat. Genet. *22*, 323–324. https://doi.org/10.1038/11887.

Dobin, A., Davis, C.A., Schlesinger, F., Drenkow, J., Zaleski, C., Jha, S., Batut, P., Chaisson, M., and Gingeras, T.R. (2013). STAR: ultrafast universal RNA-seq aligner. Bioinformatics *29*, 15–21. https://doi.org/10.1093/bioinformatics/bts635.

Evans, M.J., Cabral, L.J., Stephens, R.J., and Freeman, G. (1975). Transformation of alveolar type 2 cells to type 1 cells following exposure to NO2. Exp. Mol. Pathol. *22*, 142–150. https://doi.org/10.1016/0014-4800(75)90059-3.

Fischer, J., Jung, N., Robinson, N., and Lehmann, C. (2015). Sex differences in immune responses to infectious diseases. Infection *43*, 399–403. https://doi.org/10.1007/s15010-015-0791-9.

Galbadage, T., Peterson, B.M., Awada, J., Buck, A.S., Ramirez, D.A., Wilson, J., and Gunasekera, R.S. (2020). Systematic review and meta-analysis of sex-specific COVID-19 clinical outcomes. Front. Med. *7*, 348. https://doi.org/10.3389/fmed.2020.00348.

Heffernan, D.S., Dossett, L.A., Lightfoot, M.A., Fremont, R.D., Ware, L.B., Sawyer, R.G., and May, A.K. (2011). Gender and acute respiratory distress syndrome in critically injured adults: a prospective study. J. Trauma *71*, 878–883. discussion 883-885. https://doi.org/10.1097/TA.0b013e31822c0d31.

Huang, X., Pearce, R., and Zhang, Y. (2020). De novo design of protein peptides to block association of the SARS-CoV-2 spike protein with human ACE2. Aging (Albany NY) *12*, 11263–11276. https://doi.org/10.18632/aging.103416.

Imai, Y., Kuba, K., Rao, S., Huan, Y., Guo, F., Guan, B., Yang, P., Sarao, R., Wada, T., Leong-Poi, H., et al. (2005). Angiotensin-converting enzyme 2 protects from severe acute lung failure. Nature *436*, 112–116. https://doi.org/10.1038/nature03712.

Johnston, C.M., Lovell, F.L., Leongamornlert, D.A., Stranger, B.E., Dermitzakis, E.T., and Ross, M.T. (2008). Large-scale population study of human cell lines indicates that dosage compensation is virtually complete. PLoS Genet. *4*, e9. https://doi.org/10.1371/journal.pgen.0040009.

Kaltofen, T., Haase, M., Thome, U.H., and Laube, M. (2015). Male sex is associated with a reduced alveolar epithelial sodium transport. PLoS One *10*, e0136178. https://doi.org/10.1371/journal.pone.0136178.

Katsura, H., Sontake, V., Tata, A., Kobayashi, Y., Edwards, C.E., Heaton, B.E., Konkimalla, A., Asakura, T., Mikami, Y., Fritch, E.J., et al. (2020). Human lung stem cell-based alveolospheres provide insights into SARS-CoV-2-mediated interferon responses and pneumocyte dysfunction. Cell Stem Cell *27*, 890–904.e8. https://doi.org/10.1016/j.stem.2020.10.005.

Katzen, J., and Beers, M.F. (2020). Contributions of alveolar epithelial cell quality control to pulmonary fibrosis. J. Clin. Invest. *130*, 5088–5099. https://doi.org/10.1172/JCI139519.

Kawano-Dourado, L., Glassberg, M.K., Assayag, D., Borie, R., and Johannson, K.A. (2021). Sex and gender in interstitial lung diseases. Eur. Respir. Rev. *30*, 210105. https://doi.org/10.1183/16000617.0105-2021.

Klein, S.L., and Flanagan, K.L. (2016). Sex differences in immune responses. Nat. Rev. Immunol. *16*, 626–638. https://doi.org/10.1038/nri.2016.90.

Kohlmaier, A., Savarese, F., Lachner, M., Martens, J., Jenuwein, T., and Wutz, A. (2004). A chromosomal memory triggered by Xist regulates histone methylation in X inactivation. PLoS Biol. *2*, E171. https://doi.org/10.1371/journal.pbio.0020171.

Lau, E.S., McNeill, J.N., Paniagua, S.M., Liu, E.E., Wang, J.K., Bassett, I.V., Selvaggi, C.A., Lubitz, S.A., Foulkes, A.S., and Ho, J.E. (2021). Sex differences in inflammatory markers in patients hospitalized with COVID-19 infection: insights from the MGH COVID-19 patient registry. PLoS One *16*, e0250774. https://doi.org/10.1371/journal.pone.0250774.

Marahrens, Y., Panning, B., Dausman, J., Strauss, W., and Jaenisch, R. (1997). Xist-deficient mice are defective in dosage compensation but not spermatogenesis. Genes Dev. *11*, 156–166.

McCoy, D.M., Salome, R.G., Kusner, D.J., Iyar, S.S., and Mallampalli, R.K. (1999). Identification of sex-specific differences in surfactant synthesis in rat lung. Pediatr. Res. *46*, 722–730. https://doi.org/10.1203/00006450-199912000-00003.

McNicholas, B.A., Madotto, F., Pham, T., Rezoagli, E., Masterson, C.H., Horie, S., Bellani, G., Brochard, L., and Laffey, J.G.; LUNG SAFE Investigators and the ESICM Trials Group (2019). Demographics, management and outcome of females and males with acute respiratory distress syndrome in the LUNG SAFE prospective cohort study. Eur. Respir. J. *54*, 1900609. https://doi.org/10.1183/13993003.00609-2019.

Mekhoubad, S., Bock, C., de Boer, A.S., Kiskinis, E., Meissner, A., and Eggan, K. (2012). Erosion of dosage compensation impacts human iPSC disease modeling. Cell Stem Cell *10*, 595–609. https://doi.org/10.1016/j.stem.2012.02.014.

Parimon, T., Yao, C., Stripp, B.R., Noble, P.W., and Chen, P. (2020). Alveolar epithelial type II cells as drivers of lung fibrosis in idiopathic pulmonary fibrosis. Int. J. Mol. Sci. *21*, 2269. https://doi.org/10.3390/ijms21072269.

Payer, B., and Lee, J.T. (2008). X chromosome dosage compensation: how mammals keep the balance. Annu. Rev. Genet. *42*, 733–772. https://doi.org/10.1146/annurev.genet.42.110807.091711.

Peckham, H., de Gruijter, N.M., Raine, C., Radziszewska, A., Ciurtin, C., Wedderburn, L.R., Rosser, E.C., Webb, K., and Deakin, C.T. (2020). Male sex identified by global COVID-19 meta-analysis as a risk factor for death and ITU admission. Nat. Commun. *11*, 6317. https://doi.org/10.1038/s41467-020-19741-6.

Penny, G.D., Kay, G.F., Sheardown, S.A., Rastan, S., and Brockdorff, N. (1996). Requirement for Xist in X chromosome inactivation. Nature *379*, 131–137. https://doi.org/10.1038/379131a0.

Plath, K., Fang, J., Mlynarczyk-Evans, S.K., Cao, R., Worringer, K.A., Wang, H., de la Cruz, C.C., Otte, A.P., Panning, B., and Zhang, Y. (2003). Role of histone H3 lysine 27 methylation in X inactivation. Science *300*, 131–135. https://doi.org/10.1126/science.1084274.

Pyfrom, S., Paneru, B., Knox, J.J., Cancro, M.P., Posso, S., Buckner, J.H., and Anguera, M.C. (2021). The dynamic epigenetic regulation of the inactive X chromosome in healthy human B cells is dysregulated in lupus patients. Proc. Natl. Acad. Sci. USA *118*. e2024624118. https://doi.org/10.1073/pnas.2024624118.

Scully, E.P., Haverfield, J., Ursin, R.L., Tannenbaum, C., and Klein, S.L. (2020). Considering how biological sex impacts immune responses and COVID-19 outcomes. Nat. Rev. Immunol. *20*, 442–447. https://doi.org/10.1038/s41577-020-0348-8.

Simard, M., Provost, P.R., and Tremblay, Y. (2006). Sexually dimorphic gene expression that overlaps maturation of type II pneumonocytes in fetal mouse lungs. Reprod. Biol. Endocrinol. *4*, 25. https://doi.org/10.1186/1477-7827-4-25.

Syrett, C.M., Sindhava, V., Hodawadekar, S., Myles, A., Liang, G., Zhang, Y., Nandi, S., Cancro, M., Atchison, M., and Anguera, M.C. (2017). Loss of Xist RNA from the inactive X during B cell development is restored in a dynamic YY1-dependent two-step process in activated B cells. PLoS Genet. *13*, e1007050. https://doi.org/10.1371/journal.pgen.1007050.

Syrett, C.M., Sindhava, V., Sierra, I., Dubin, A.H., Atchison, M., and Anguera, M.C. (2018). Diversity of epigenetic features of the inactive X-chromosome in NK cells, dendritic cells, and macrophages. Front. Immunol. *9*, 3087. https://doi.org/10.3389/fimmu.2018.03087.

Syrett, C.M., Paneru, B., Sandoval-Heglund, D., Wang, J., Banerjee, S., Sindhava, V., Behrens, E.M., Atchison, M., and Anguera, M.C. (2019). Altered X-chromosome inactivation in T cells may promote sex-biased autoimmune diseases. JCI Insight *4*, e126751. https://doi.org/10.1172/jci.insight.126751.

Takahashi, T., Ellingson, M.K., Wong, P., Israelow, B., Lucas, C., Klein, J., Silva, J., Mao, T., Oh, J.E., Tokuyama, M., et al. (2020). Sex differences in immune responses that underlie COVID-19 disease outcomes. Nature *588*, 315–320. https://doi.org/10.1038/s41586-020-2700-3.

Tukiainen, T., Villani, A.C., Yen, A., Rivas, M.A., Marshall, J.L., Satija, R., Aguirre, M., Gauthier, L., Fleharty, M., Kirby, A., et al. (2017). Landscape of X chromosome inactivation across human tissues. Nature *550*, 244–248. https://doi.org/10.1038/nature24265.

Vaughan, A.E., Brumwell, A.N., Xi, Y., Gotts, J.E., Brownfield, D.G., Treutlein, B., Tan, K., Tan, V., Liu, F.C., Looney, M.R., et al. (2015). Lineage-negative progenitors mobilize to regenerate lung epithelium after major injury. Nature *517*, 621–625. https://doi.org/10.1038/nature14112.

Wang, J., Syrett, C.M., Kramer, M.C., Basu, A., Atchison, M.L., and Anguera, M.C. (2016). Unusual maintenance of X chromosome inactivation predisposes female lymphocytes for increased expression from the inactive X. Proc. Natl. Acad. Sci. USA *113*, E2029–E2038. https://doi.org/10.1073/pnas.1520113113.

Weiner, A.I., Jackson, S.R., Zhao, G., Quansah, K.K., Farshchian, J.N., Neupauer, K.M., Littauer, E.Q., Paris, A.J., Liberti, D.C., Scott Worthen, G., et al. (2019). Mesenchyme-free expansion and transplantation of adult alveolar progenitor cells: steps toward cell-based regenerative therapies. NPJ Regen. Med. *4*, 17. https://doi.org/10.1038/s41536-019-0080-9.

Wenham, C., Smith, J., and Morgan, R.; Gender and COVID-19 Working Group (2020). COVID-19: the gendered impacts of the outbreak. Lancet *395*, 846–848. https://doi.org/10.1016/S0140-6736(20)30526-2.

Xi, Y., Kim, T., Brumwell, A.N., Driver, I.H., Wei, Y., Tan, V., Jackson, J.R., Xu, J., Lee, D.K., Gotts, J.E., et al. (2017). Local lung hypoxia determines epithelial fate decisions during alveolar regeneration. Nat. Cell Biol. *19*, 904–914. https://doi.org/10.1038/ncb3580.

Yildirim, E., Kirby, J.E., Brown, D.E., Mercier, F.E., Sadreyev, R.I., Scadden, D.T., and Lee, J.T. (2013). Xist RNA is a potent suppressor of hematologic cancer in mice. Cell *152*, 727–742. https://doi.org/10.1016/j.cell.2013.01.034.

Zhao, J., Sun, B.K., Erwin, J.A., Song, J.J., and Lee, J.T. (2008). Polycomb proteins targeted by a short repeat RNA to the mouse X chromosome. Science *322*, 750–756. https://doi.org/10.1126/science.1163045.

Zhou, Y., Zhou, B., Pache, L., Chang, M., Khodabakhshi, A.H., Tanaseichuk, O., Benner, C., and Chanda, S.K. (2019). Metascape provides a biologist-oriented resource for the analysis of systems-level datasets. Nat. Commun. *10*, 1523. https://doi.org/10.1038/s41467-019-09234-6.

Zou, Z., Yan, Y., Shu, Y., Gao, R., Sun, Y., Li, X., Ju, X., Liang, Z., Liu, Q., Zhao, Y., et al. (2014). Angiotensin-converting enzyme 2 protects from lethal avian influenza A H5N1 infections. Nat. Commun. *5*, 3594. https://doi.org/10.1038/ncomms4594.

Stem Cell Reports, Volume *18*

Supplemental Information

Unusual X chromosome inactivation maintenance in female alveolar type 2 cells is correlated with increased numbers of X-linked escape genes and sex-biased gene expression

Isabel Sierra, Sarah Pyfrom, Aaron Weiner, Gan Zhao, Amanda Driscoll, Xiang Yu, Brian D. Gregory, Andrew E. Vaughan, and Montserrat C. Anguera

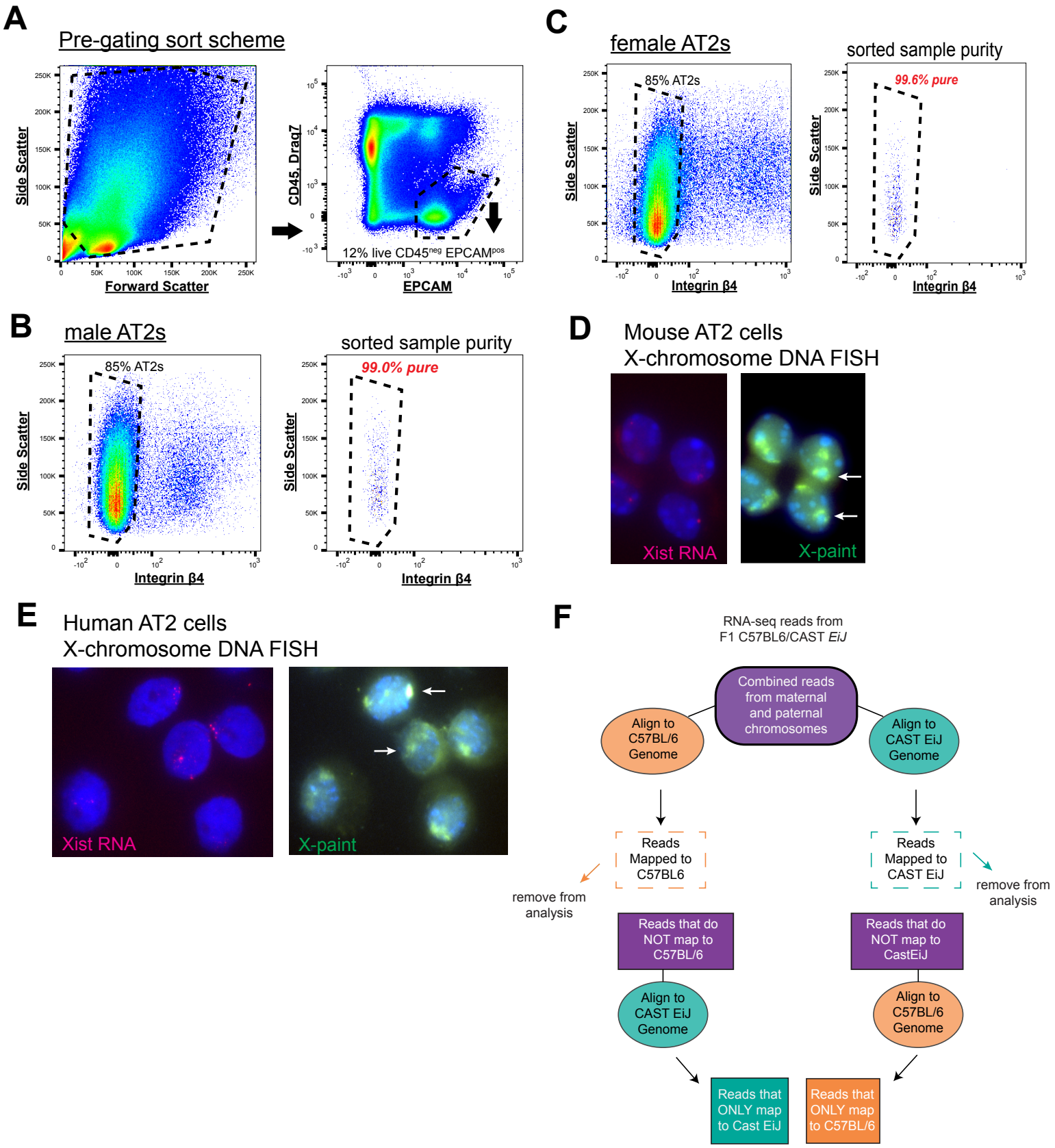

Supplemental Figure 1

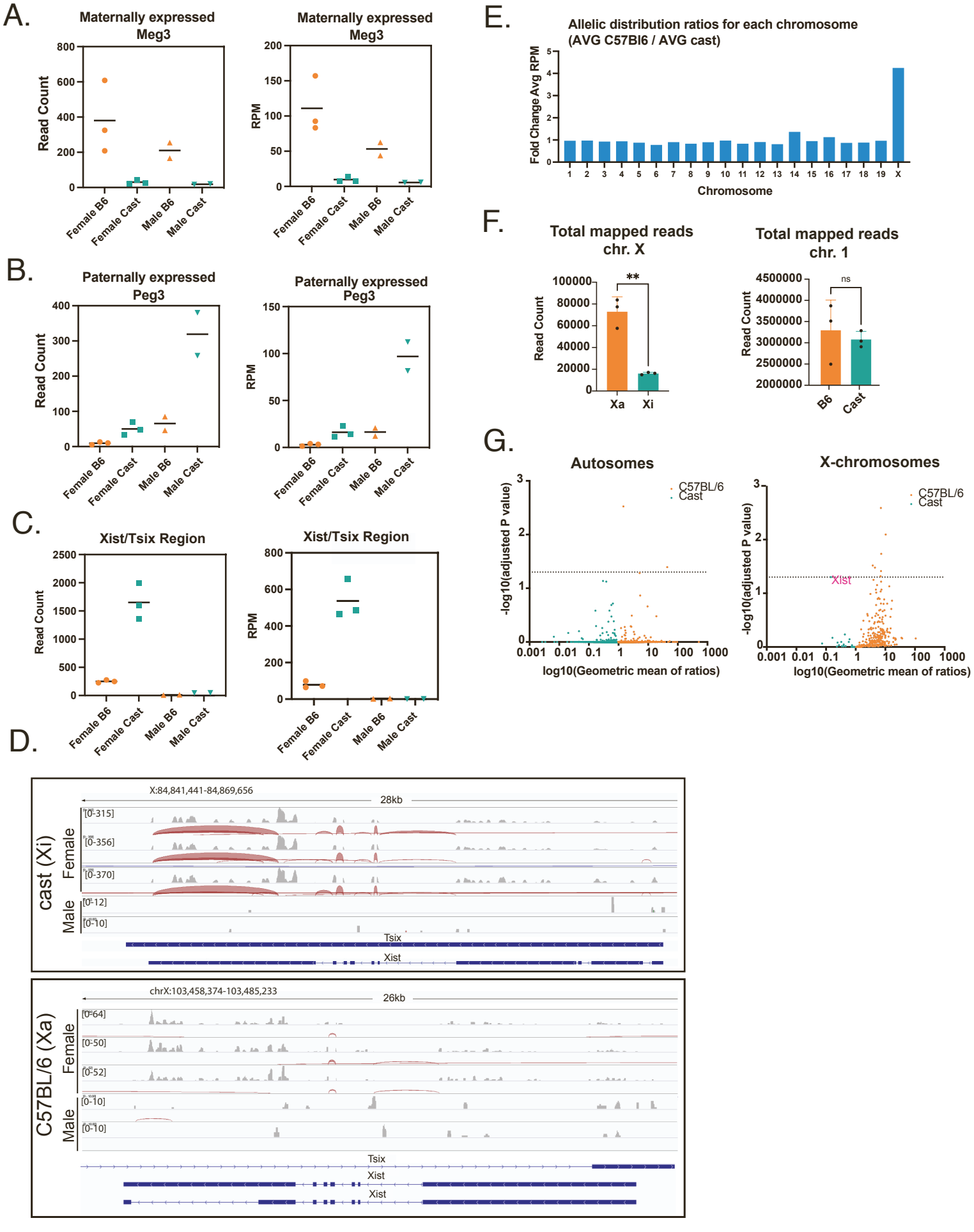

Supplemental Figure 2

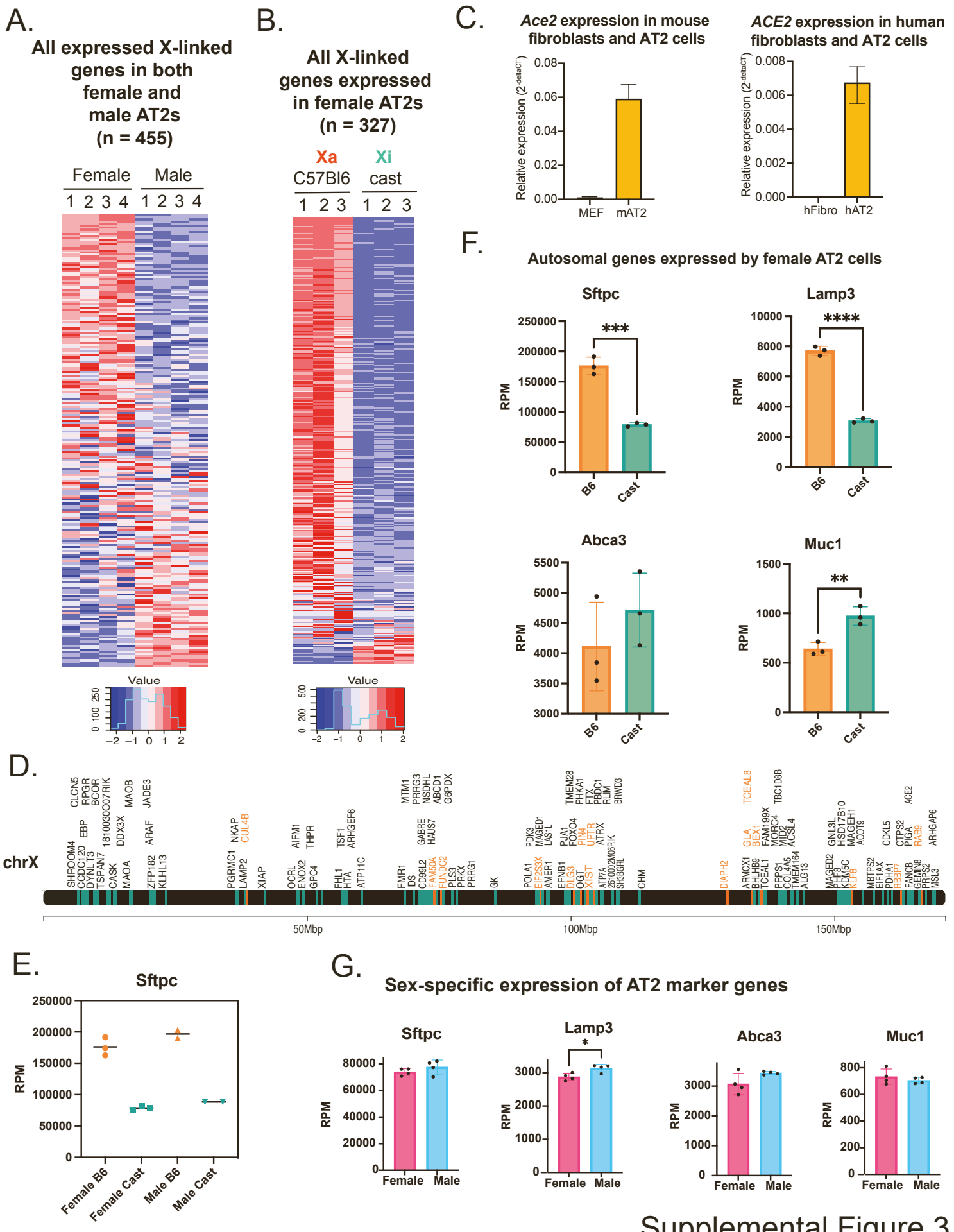

Supplemental Figure 3

A.

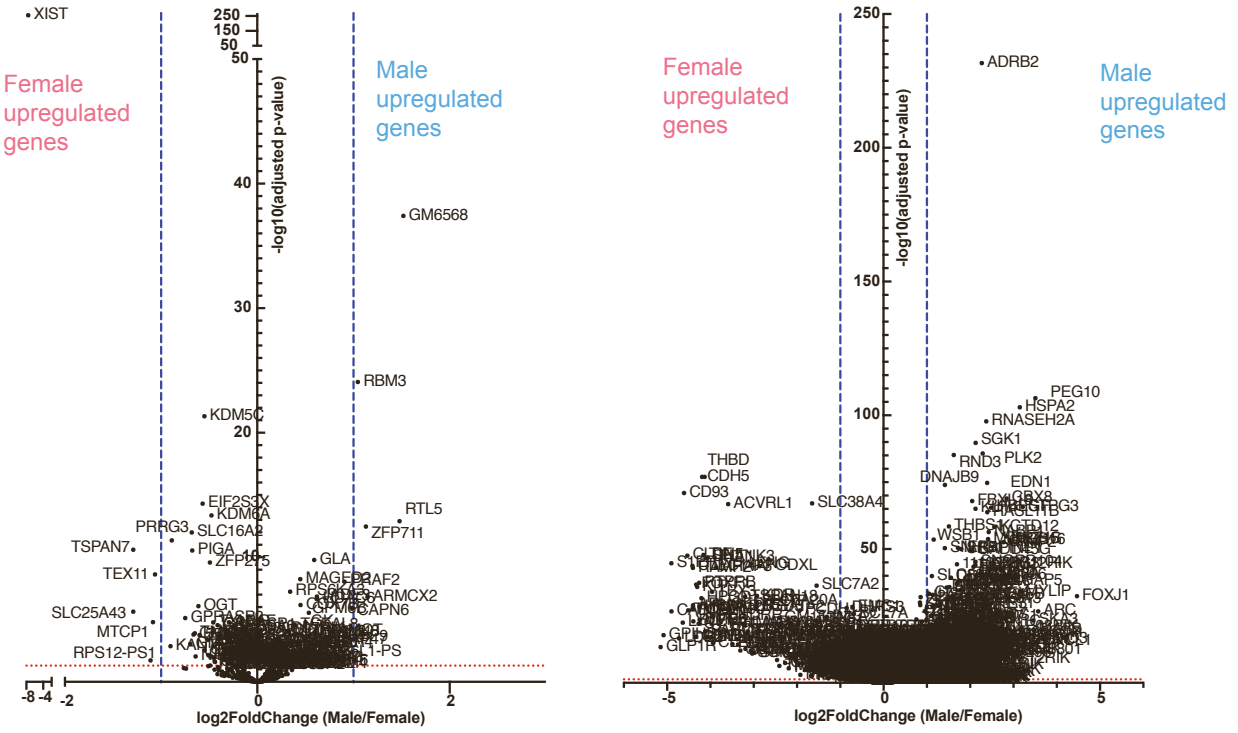

B.

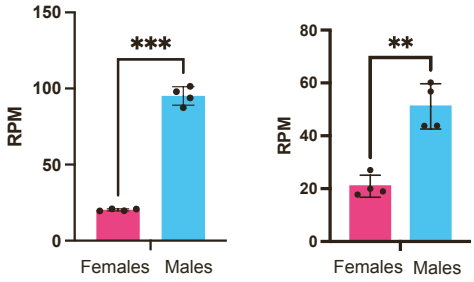

C.

Sex-specific Gene Ontology Analyses

Female-specific upregulation Category	Count	Log10(P)
autophagy	43	-8.05
protein modification by small protein conjugation or removal	85	-8.04
positive regulation of catabolic process	64	-6.46
phosphatidylinositol biosynthetic process	21	-6.17
Herpes simplex virus 1 infection	56	-5.43

Male-specific Category	Count	Log10(P)
Nonsense Mediated Decay independent of the Exon Junction Complex	43	-33.54
mRNA processing	51	-9.02
Parkinson disease	36	-8.72
Cholesterol biosynthesis	8	-7.16
nucleobase-containing compound biosynthetic process	56	-6.93

D.

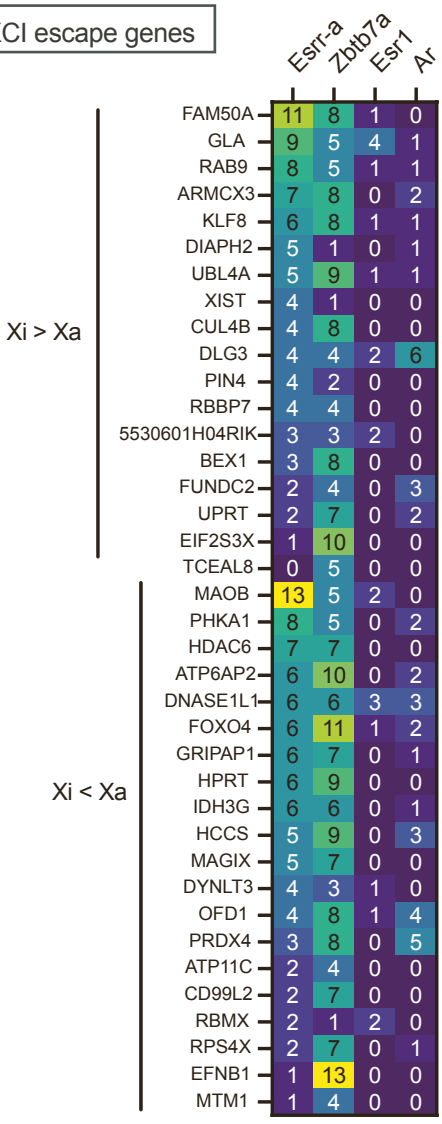

Supplemental Figure 4

Supplementary Figure 1. AT2 cell isolation for imaging and allele-specific transcriptional profiling. A. FACS sorting scheme for AT2 isolation. Total lung digest is pre-gated on forward and side scatter and live (DRAQ7^{neg}), CD45^{neg}, EPCAM^{pos}. B-C. Within the gates shown in A, male (B) and female (C) AT2s were further defined by gating on integrin β4^{neg}. Sort purity was extremely high, >99% EPCAM^{pos} integrin β4^{neg} for both male and female sorts. D-E. DNA FISH for the X chromosomes in mouse (D) and (E) human AT2 cells. The same field is shown for Xist RNA FISH (left) and X-paint (right). White arrows indicated the Xi, based on overlapping Xist RNA signal. (F). Schematic diagram showing the overview for the alignment to *mus musculus* and *mus castaneus* genomes for the allele-specific RNAseq pipeline.

Supplementary Figure 2. Allele-specific RNAseq profiling of female and male AT2 cells. (A) Allele-specific RNAseq analyses of imprinted genes: *Meg3*, *Peg3*, and *Xist.* Read counts and normalized RPM values for each gene (A) *Meg3* (chr.12), (B) *Peg3* (Chr.7), and (C) *Xist/Tsix* region (chr.X) are shown. The transcript levels for each allele in female and male AT2 cells are shown. (D) IGV coverage (grey) and splice junction (red) tracks showing allele-specific alignment of unique reads that map to the *Xist* and *Tsix* region in female and male F1 mus x cast mice. Note that these reads are not strand-specific, thus we cannot distinguish whether the reads from C57BL/6 (Xa) are Tsix or Xist transcripts. (E) Allelic distribution of mapped reads for all chromosomes in female AT2 cells. The fold change of average RPM values (shown as the ratio of C57Bl6/cast RPM) for all autosomes and X chromosome. (F) The allelic distribution for total mapped reads for each allele, for the X chromosome (Xa or Xi) and chromosome 1

(C57BL/6 or cast). Statistical significance determined using unpaired t-test, ** $p < 0.005$; ns, not significant. (G) The geometric mean of gene expression ratios for allelic expression in female F1 mus x cast mice, for each autosomal gene (left) and X-linked gene (right). C57BL/6 ratios in orange; cast ratios in teal. P values were calculated using ratio paired t-tests and corrected for multiple comparisons using the Holm-Sidak method (alpha = 0.05).

Supplementary Figure 3. Sex-specific and allele-specific profiling of X-linked and AT2 marker genes. (A) Expression of all X-linked genes (n=455 genes) in female and male AT2 cells. Heatmap showing z-score normalized expression the X-linked genes in female (n = 4) and male (n = 4) AT2 samples. Genes were considered 'expressed' if RPM > 1 across all 4 female samples. (B) Allele-specific expression of X-linked genes in female AT2 cells. Heatmap showing allele-specific expression from the Xa (C57BL/6) or the Xi (cast) for all expressed X-linked genes containing a SNP (n=327 genes). (C) Ace2/ACE2 expression in fibroblasts and AT2 cells from mice and humans using qPCR. (D) Location of AT2-specific XCI escape genes across the X-chromosome. Green locations indicate genes that have higher expression from the Xa; orange locations indicate genes that have higher expression from the Xi. (E) Allele-specific expression of *Sftpc* in female and male AT2 cells. (F) Allele-specific expression of known AT2 marker genes *Sftpc, Lamp3, Abca3,* and *Muc1* in female AT2 cells. Statistical significance determined using unpaired t-test, *** $p < 0.0005$; **** $p < 0.00005$. (G) Sex-specific expression of *Sftpc, Lamp3, Abca3, Muc1* in female and male AT2 cells. Statistical significance determined using unpaired t-test, * $p < 0.005$.

Supplementary Figure 4. (A) Volcano plot of X-linked (left) and autosomal (right) genes upregulated in female and male AT2 cells. Blue dashed lines indicate the cutoff for log2 fold change of expression (x-axis) and the y-axis is the adjusted p-value for significance of differential expression. (B) Sex-specific expression (diploid mapped reads) for two autosomal genes (*Adrb2, Gnas*) upregulated in male AT2 cells. Statistical significance determined using student's t-test. (C) Gene ontology analyses for pathways upregulated in female (top) or male (bottom) AT2 cells. Top 5 GO categories are shown; complete lists are shown in **Supplemental Table 3**. (D) Numbers of binding sites for hormone (Ar, Esr1) and nuclear receptor (Esrr-alpha and Zbtb7a) transcription factors in promotor regions (2kb of TSS) of two groups of XCI escape genes expressed in AT2 cells: Xi > Xa denotes genes where there is more expression from the Xi; Xi < Xa denotes genes where there is more expression from Xa.

Supplemental Table 1: List of XCI escape genes in female AT2s that escape according to the binominal confidence interval calculation. The allelic ratio (Xi/Xa) is shown for each XCI escape gene.

Supplemental Table 2: All expressed genes (genome-wide) for male and female replicates (n=4), showing total read count (first tab) and RPM values (second tab) for each replicate sample. Gene ID, gene name, and chromosome are also shown.

Supplemental Tables 3a, 3b, 3c: Gene Ontology (GO) Analyses for genes upregulated in female AT2s (Table 3a), upregulated in male AT2s (Table 3b), and XCI escape genes (Table 3c). Top 20 clusters with their representative enriched terms (one per cluster). "Count" is the number of genes in the user-provided lists with membership in the given ontology term. "%" is the percentage of all of the user-provided genes that are found in the given ontology term (only input genes with at least one ontology term annotation are included in the calculation). "Log10(P)" is the p-value in log base 10. "Log10(q)" is the multi-test adjusted p-value in log base 10.

Supplemental Procedures

Mice

$Xist^{2lox/2lox}$ animals (129Sv/Jae) were a gift of R. Jaenisch (Csankovszki *et al.*, 1999), and live animals were kindly transferred to our colony from J.T.Lee. $Xist^{2lox/2lox}$ mice were backcrossed to C57Bl6 background for 10 generations, and then mated to B-actin Cre Recombinase mice (strain 033984; Jackson labs). F1 mus/cast mice (Xa $^{Xist\ KO}$ Xi) were generated by mating $Xist^{+/KO}$ females with wild-type *Mus castaneus* (*Cast*) males. F1 mus/cast $Xist^{+/KO}$ females from this mating always inactivate the paternal *cast* X chromosome. Mice were screened by PCR primers for Cre-Recombinase and $Xist^{2lox}$ alleles using previously published primer sets(Yildirim *et al.*, 2013). Animal experiments were approved by the University of Pennsylvania Institutional Animal Care and Use Committee (IACUC). Euthanasia via carbon dioxide was used for animal sacrifice prior to lung isolation.

Immunofluorescence (IF)

For IF analyses, slide locations were recorded for Xist RNA FISH images first, and then slides were blocked for 30 min in blocking buffer (PBS with 0.2% Tween-20 and 5% BSA) and then incubated for 2 hours at room temperature with respective primary antibodies (1:100 dilution): H3K27me3 (39155, Active Motif); H2AK119-ubiquitin (8240, Cell Signaling). Slides were incubated with the appropriate FITC conjugated secondary antibody, washed, then imaged at the corresponding locations using a fluorescence microscope.

Read alignment for allele-specific RNA sequencing

500,000 to 1 million AT2 cells were sorted from male and female F1 mus x cast mice, and placed in Trizol. Total RNA isolations were performed following manufacturers protocol. We used the TruSeq Stranded mRNA Library Prep (20020594, Illumina), and libraries were checked for quality using TapeStation, pooled, and subsequently run on the Illumina NextSeq 500 using 75bp single-end reads. Total number of reads per sample varied between 30-80 million. For allele-specific mapping, RNA-seq reads were first aligned to the Cast genome using STAR (v2.6.0a) with default parameters, except for the outSAMunmapped flag, which was set to Within KeepPairs to allow for unmapped reads to be extracted from alignment output. Unmapped reads were extracted using samtools and converted to Fastq format using bamToFastq. These reads were then aligned to the C57Bl/6 genome using STAR with the outFilterMultimapNmax flag set to 1 to filter out reads that mapped to more than one locus. With the output from this second alignment, HTSeq-count (v0.10.0) was used to count allele-specific reads mapping to genes in the

C57Bl/6 genome. To quantify read counts from the Cast genome, the same strategy was employed, except reads were first mapped to the C57Bl/6 genome and unmapped reads were then mapped to the Cast genome.

Hormone receptor binding-site analysis

Bed files (MA0007.3, MA0141.3, MA0592.3, MA0112.3, MA0258.2, MA0750.2) containing select predicted transcription factors binding sites (TFBS) in the mm10 genome were downloaded from http://expdata.cmmt.ubc.ca/JASPAR/downloads/UCSC_tracks/2022/mm10/. Bedfiles were merged and intersected with a 4kb region around the transcriptional start site (TSS) of mm10 genes using the Bedtools Suite (Quinlan and Hall, 2010).

Supplemental References

Camelo, A., Dunmore, R., Sleeman, M.A., and Clarke, D.L. (2014). The epithelium in idiopathic pulmonary fibrosis: breaking the barrier. Front Pharmacol *4*, 173. 10.3389/fphar.2013.00173.
Chapman, H.A., Li, X., Alexander, J.P., Brumwell, A., Lorizio, W., Tan, K., Sonnenberg, A., Wei, Y., and Vu, T.H. (2011). Integrin alpha6beta4 identifies an adult distal lung epithelial population with regenerative potential in mice. J Clin Invest *121*, 2855-2862. 10.1172/JCI57673.
Dobin, A., Davis, C.A., Schlesinger, F., Drenkow, J., Zaleski, C., Jha, S., Batut, P., Chaisson, M., and Gingeras, T.R. (2013). STAR: ultrafast universal RNA-seq aligner. Bioinformatics *29*, 15-21. 10.1093/bioinformatics/bts635.
Evans, M.J., Cabral, L.J., Stephens, R.J., and Freeman, G. (1975). Transformation of alveolar type 2 cells to type 1 cells following exposure to NO2. Exp Mol Pathol *22*, 142-150. 10.1016/0014-4800(75)90059-3.
Huang, X., Pearce, R., and Zhang, Y. (2020). De novo design of protein peptides to block association of the SARS-CoV-2 spike protein with human ACE2. Aging (Albany NY) *12*, 11263-11276. 10.18632/aging.103416.
Leong-Poi, H., et al. (2005b). Angiotensin-converting enzyme 2 protects from severe acute lung failure. Nature *436*, 112-116. 10.1038/nature03712.
Katsura, H., Sontake, V., Tata, A., Kobayashi, Y., Edwards, C.E., Heaton, B.E., Konkimalla, A., Asakura, T., Mikami, Y., Fritch, E.J., et al. (2020). Human Lung Stem

Cell-Based Alveolospheres Provide Insights into SARS-CoV-2-Mediated Interferon Responses and Pneumocyte Dysfunction. Cell Stem Cell *27*, 890-904 e898. 10.1016/j.stem.2020.10.005.
Lau, E.S., McNeill, J.N., Paniagua, S.M., Liu, E.E., Wang, J.K., Bassett, I.V., Selvaggi, C.A., Lubitz, S.A., Foulkes, A.S., and Ho, J.E. (2021). Sex differences in inflammatory markers in patients hospitalized with COVID-19 infection: Insights from the MGH COVID-19 patient registry. PLOS ONE *16*, e0250774. 10.1371/journal.pone.0250774.
Quinlan, A.R., and Hall, I.M. (2010). BEDTools: a flexible suite of utilities for comparing genomic features. Bioinformatics *26*, 841-842. 10.1093/bioinformatics/btq033.
Zhou, Y., Zhou, B., Pache, L., Chang, M., Khodabakhshi, A.H., Tanaseichuk, O., Benner, C., and Chanda, S.K. (2019). Metascape provides a biologist-oriented resource for the analysis of systems-level datasets. Nat Commun *10*, 1523. 10.1038/s41467-019-09234-6.